Appendix A

Convergence Tests

All DFT results presented in this work have been obtained within the FP-(L)APW+lo method (cf. Chapter 3) as implemented in the WIEN2k code. Besides the error introduced by the only approximate exchange-correlation functional the accuracy of the results does also depend on several other computational parameters, which have to be carefully tested for every new investigated problem. Within the (L)APW+lo method the most important parameters that have to be considered are the muffin-tin radii, R_{MT}, the planewave cutoff for the expansion of the wave function in the interstitial, $E_{\mathrm{max}}^{\mathrm{wf}}$, and the **k**-point mesh for the sampling of the Brillouin zone. The remaining parameters have usually a much smaller influence on the computational time as well as on the accuracy and are therefore always set to rather conservative values.

The muffin-tin radii have to be carefully chosen at the beginning of each new project. Since the muffin-tin spheres are not allowed to overlap, the smallest possible nearest neighbor distance has to be estimated to obtain an upper limit for R_{MT}. With respect to this upper limit the muffin-tin radii should always be chosen as large as possible to minimize the interstitial region, which reduces the number of required planewaves and thus the computational cost. Since in the (L)APW+lo method the core states are only treated within the muffin-tin spheres, the muffin-tin radius has to be large enough to include the spatial extension of the core states. Thus, heavier atoms usually require a larger R_{MT} than lighter atoms. Absolute energies of the same system obtained with different muffin-tin radii are not comparable.

The planewave cutoff for the expansion of the wave function in the interstitial, $E_{\mathrm{max}}^{\mathrm{wf}}$, determines the number of basis functions. With increasing $E_{\mathrm{max}}^{\mathrm{wf}}$ the basis set can be systematically improved by an increasing number of planewaves. Since it is not possible to include an infinite number of basis functions, the expansion has to be truncated by a suitable choice of $E_{\mathrm{max}}^{\mathrm{wf}}$. The size of the required basis set depends on the aspired accuracy, as well as on the muffin-tin radii and the investigated system. Usually it is much more efficient to test the basis set with respect to the investigated physical quantity instead of the total energy of the system.

In the present work careful tests have been performed to check the convergence of the

results with respect to the applied basis set and **k**-point mesh. In all test calculations only the PBE exchange-correlation functional has been used, since the convergence behavior is not expected to depend much on the choice of the exchange-correlation functional. In the following, tests regarding the PdO surfaces, the adsorption on the Pd(100) surface and the $(\sqrt{5} \times \sqrt{5})R27^\circ$ surface oxide structure, as well as the molecular binding energies of O_2, CO and CO_2 are presented. For the palladium and palladium oxide bulk systems convergence tests with respect to the different parameters have already been performed previously [115].

A.1 PdO Surfaces

To determine the required basis set and number of **k**-points the convergence of the surface energy γ as defined in Eq. (6.4) is tested, since the surface energy is needed to compare the stability of the different PdO surface terminations (cf. Chapter 6). As discussed in Ref. [115] the muffin-tin radii are set to $R_{\mathrm{MT}}^{\mathrm{O}} = 1.3\,\mathrm{bohr}$ for oxygen and $R_{\mathrm{MT}}^{\mathrm{Pd}} = 1.8\,\mathrm{bohr}$ for palladium. The same muffin-tin radii have to be used in all calculations entering the surface energy, i.e. the PdO surface slabs, the PdO bulk and the Pd bulk calculations. Also referring to Ref. [115] the wave function expansion inside the muffin-tin spheres is considered up to $l_{\mathrm{max}}^{\mathrm{wf}} = 12$ and the potential expansion up to $l_{\mathrm{max}}^{\mathrm{pot}} = 6$ and the energy cutoff for the planewave representation of the potential in the interstitial region is set to $E_{\mathrm{max}}^{\mathrm{pot}} = 196\,\mathrm{Ry}$.

Thus, the remaining parameters that need to be tested are the planewave cutoff for the expansion of the wave function in the interstitial, $E_{\mathrm{max}}^{\mathrm{wf}}$, and the number of **k**-points. Since the surface calculations are performed within the supercell approach additionally the number of layers and the vacuum thickness have to tested. The convergence behavior of the different parameters is usually independent, i.e. one parameter can be tested while setting the others to reasonable but not necessarily converged values. In all test calculations only one terminations for each low-index surface is used in the bulk truncated geometry without any relaxation.

In Fig. A.1 the dependence of the surface energy γ on the planewave cutoff $E_{\mathrm{max}}^{\mathrm{wf}}$ is illustrated for the five different low index surfaces. For the PdO(100)-PdO, PdO(101) and the PdO(110)-Pd terminations supercells containing 3 layer-thick slabs are used, for the PdO(001)-Pd and PdO(111)-Pd terminations the slabs consist of 5 layers. For all terminations the vacuum region is larger than 20 Å. The Monkhorst-Pack grids and corresponding numbers of **k**-points in the irreducible part of the Brillouin zone applied in the planewave cutoff tests for the different terminations are listed in Tab. A.1. Regarding the rather small scale of the y-axes of the different plots in Fig. A.1 it can be seen that the surface energy shows a rather fast convergence with respect to the planewave cutoff. Already at a value of $E_{\mathrm{max}}^{\mathrm{wf}} = 17\,\mathrm{Ry}$ the surface energies are converged within 3–4 $\mathrm{meV/Å^2}$ compared to the best obtained value.

The convergence of the surface energy with respect to the number of **k**-points in the irreducible part of the Brillouin zone is shown in Fig. A.2. The setup of the supercells

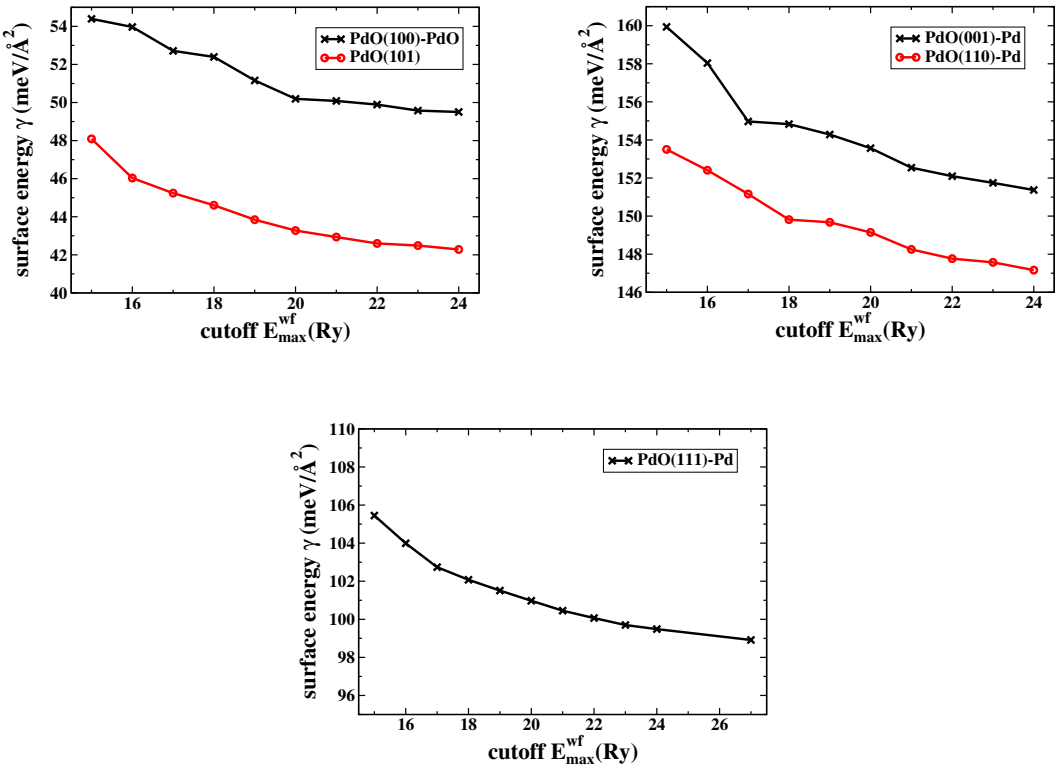

Figure A.1: Convergence of the surface energy γ with respect to the cutoff of the planewave representation of the wave function in the interstitial region, $E^{\mathrm{wf}}_{\mathrm{max}}$ for the five low-index PdO surface orientations.

PdO surface	MP grid	no. of irred. **k**-points
(100) ≡ (010)	[4×7×1]	12
(001)	[7×7×1]	16
(101) ≡ (011)	[1×3×7]	8
(110)	[4×3×1]	6
(111)	[3×5×1]	8

Table A.1: Employed Monkhorst-Pack grids during the planewave cutoff tests and corresponding number of **k**-points in the irreducible part of the Brillouin zone for the different (1×1) surface unit cells of the low-index PdO surfaces

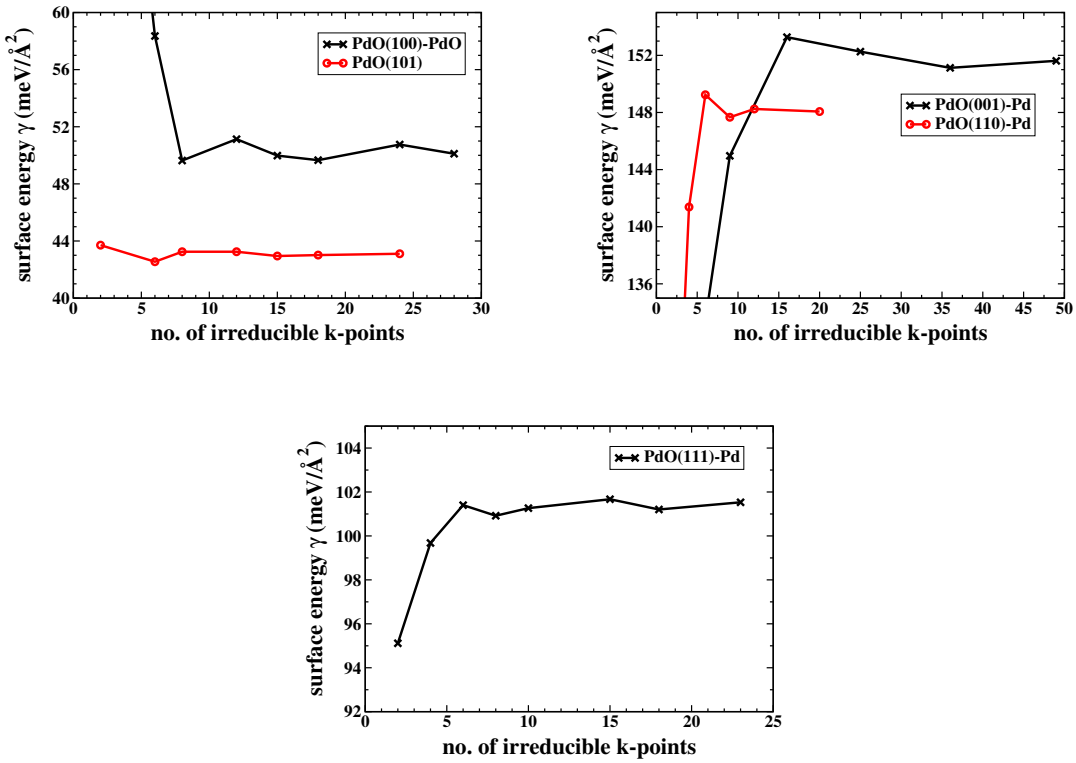

Figure A.2: Convergence of the surface energy γ with respect to the number of **k**-points in the irreducible part of the Brillouin zone for the five low-index PdO surface orientations.

is equivalent to the one used in the previous test, the planewave cutoff is set to $E_{\text{max}}^{\text{wf}} = 20\,\text{Ry}$ (since the different test calculations were performed simultaneously, this rather high value for $E_{\text{max}}^{\text{wf}}$ was chosen; considering the results of the planewave cutoff test a value of $E_{\text{max}}^{\text{wf}} = 17\,\text{Ry}$ would have been sufficient). In contrast to the very similar convergence behavior of all five terminations with respect to the planewave cutoff the convergence with respect to the number of **k**-points is not comparable for the different terminations. These differences originate from the different symmetry of the supercells representing the five terminations and the resulting different sampling of the Brillouin zone. Nevertheless it can be seen that with increasing density of the **k**-point grids the surface energy converges nicely for each of the five terminations. For the MP-grids listed in Tab. A.2 all surface energies are converged within 1–2 meV/Å^2 compared to the best obtained value.

Using the optimum number of **k**-points listed Tab. A.2 and a planewave cutoff of $E_{\text{max}}^{\text{wf}} = 20\,\text{Ry}$ the number of layers within a slab that is needed to decouple the bottom and top surfaces of the slab is tested. The results are illustrated in Fig. A.3. For all surface terminations a clear convergence of the surface energy with an increasing number of layers in the slab can be observed. For the PdO(100)-PdO termination a minimum number of 7 layers per slab is chosen, for the PdO(001)-Pd, PdO(101)

PdO surface	MP grid	no. of irred. **k**-points
(100) ≡ (010)	[3×7×1]	8
(001)	[7×7×1]	16
(101) ≡ (011)	[1×3×7]	8
(110)	[4×3×1]	6
(111)	[2×4×1]	6

Table A.2: Optimal Monkhorst-Pack grids and corresponding number of **k**-points in the irreducible part of the Brillouin zone for the different (1×1) surface unit cells of the low-index PdO surfaces. Applying these MP-grids the respective surface energies are converged within 1–2 meV/Å^2.

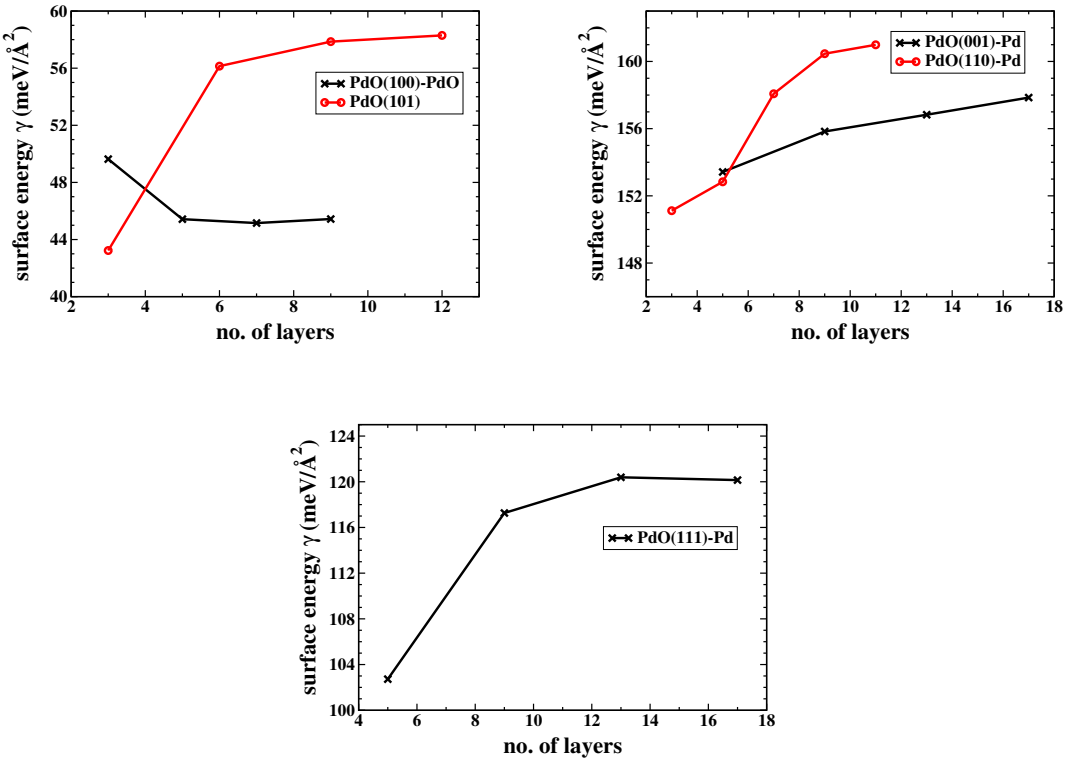

Figure A.3: Convergence of the surface energy γ with respect to the number of layers within the slab representing the five low-index PdO surface terminations.

and PdO(111)-Pd terminations at least 9 layers are used and for the PdO(110)-Pd termination the slab-thickness is set to 11 layers to achieve a convergence in the surface energy of $\approx 3\,\mathrm{meV/Å^2}$.

Since the z-length of the supercell is kept constant the vacuum will decrease with an increasing number of layers. For the largest number of layers the vacuum is still ≥ 12Å. Doubling the vacuum to $\sim 25\,$Å leads to a change in the surface energy of $\leq 1\,\mathrm{meV/Å^2}$ for any of the investigated terminations. Thus, a minimum value for the vacuum of $12\,$Å appears to be sufficient.

The presented results of the surface energies for the different PdO low-index surface terminations can therefore be considered as well converged with respect to the here discussed computational setup.

A.2 Adsorption On Pd(100) And $(\sqrt{5}\times\sqrt{5})R27°$

Similar to the tests described in the previous Section again the size of the basis set, the number of **k**-points, as well as the setup of the supercell have to be considered. Yet, instead of comparing the surface energy, here the binding energy, $\Delta\widetilde{E}^{\mathrm{bind}}_{\mathrm{O,CO@Pd}}$, as defined in Eq. (7.3) is converged with respect to these parameters, since the binding energy $\Delta\widetilde{E}^{\mathrm{bind}}_{\mathrm{O,CO@Pd}}$ is the decisive quantity in comparing the stability of the different phase within the surface phase diagram.

Since the bond length in the CO molecule is only $\sim 2.15\,$bohr the muffin-tin radius of the oxygen has to be slightly decreased compared to the PdO surface calculations and thus the muffin-tin radius of the palladium is slightly increased, yielding $R^{\mathrm{O}}_{\mathrm{MT}} = 1.0\,$bohr, $R^{\mathrm{Pd}}_{\mathrm{MT}} = 2.0\,$bohr and $R^{\mathrm{C}}_{\mathrm{MT}} = 1.0\,$bohr.

Previous work by M. Todorova [144] already provided careful tests regarding the convergence of the binding energies on the Pd(100) surface as well as on the $(\sqrt{5}\times\sqrt{5})R27°$ surface oxide with respect to the employed Monkhorst-Pack **k**-point grids. In the present work these results have been used and led to a choice of $[10\times10\times1]$ MP-grid (6 **k**-points in the irreducible part of the BZ) for the (1×1)-Pd(100) surface unit cell and respectively smaller MP-grids for the (2×2), $(2\sqrt{2}\times\sqrt{2})R45°$, $(3\sqrt{2}\times\sqrt{2})R45°$ and $(4\sqrt{2}\times\sqrt{2})R45°$ surface unit cells. For the $(\sqrt{5}\times\sqrt{5})R27°$ surface oxide structure a $[4\times4\times1]$ MP-grid is used.

Similarly the number of layers per slab in the setup of the supercell representing the Pd(100) surface is adopted from Ref. [144]. Thus all calculations concerning the Pd(100) surface are performed using 5 layer slabs and a vacuum of at least 13 Å. For the $(\sqrt{5}\times\sqrt{5})R27°$ surface oxide structure the average binding energy per oxygen atom is shown in Tab. A.3 for slabs containing 3, 5 and 7 Pd(100) layers in between the upper and lower surface oxide trilayer. It can be clearly seen that the average binding energy hardly changes in going from 3 to 5 to 7 Pd(100) layers separating the surface oxide trilayers. All initial calculations involving the $(\sqrt{5}\times\sqrt{5})R27°$ surface oxide are thus performed using 3 Pd(100) layers, only the final structures entering the surface phase diagram (cf. Chapter 7) and the lattice gas Hamiltonian (cf. Appendix C) have

	$\widetilde{E}^{\text{bind}}_{\text{O@Pd(100)}}$
$(\sqrt{5}\times\sqrt{5})R27°$–3 Pd layer	-1.195
$(\sqrt{5}\times\sqrt{5})R27°$–5 Pd layer	-1.201
$(\sqrt{5}\times\sqrt{5})R27°$–7 Pd layer	-1.203

Table A.3: Average binding energy per oxygen atom in the $(\sqrt{5}\times\sqrt{5})R27°$ surface oxide structure for slabs containing 3, 5 and 7 Pd(100) layers in between the upper and lower surface oxide trilayer. All values are in eV.

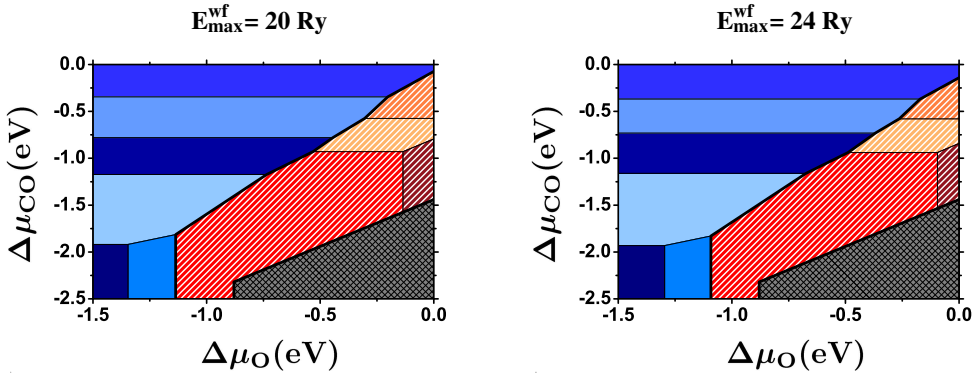

Figure A.4: Surface phase diagram for the Pd(100) surface in a constrained equilibrium with an O_2 and CO gas phase calculated using PBE exchange correlation functional. The left figure shows the results for a planewave cutoff of $E^{\text{wf}}_{\text{max}} = 20\,\text{Ry}$, the right figure for $E^{\text{wf}}_{\text{max}} = 24\,\text{Ry}$.

also been calculated using 5 Pd(100) layers in between the surface oxide trilayers.

Since in the previous work by Todorova [144] different muffin-tin radii have been used and instead of the here applied (L)APW+lo method the LAPW method has been used the results for the convergence of the binding energies with respect to the cutoff for the planewave representation of the wave function in the interstitial, $E^{\text{wf}}_{\text{max}}$, are not directly transferable. On the one hand, in the present work the smallest muffin-tin radius, which is the one for the oxygen, is smaller, so that an increase in the planewave cutoff would be expected. On the other hand, it could be shown that the (L)APW+lo method converges faster than the LAPW method [58] and thus a smaller planewave cutoff would be sufficient. Based on these considerations an initial planewave cutoff of $E^{\text{wf}}_{\text{max}} = 20\,\text{Ry}$ is chosen. Increasing the planewave cutoff up to $E^{\text{wf}}_{\text{max}} = 24\,\text{Ry}$ leads to a change in the binding energies of $\lesssim 50\,\text{meV}$ per oxygen atom resp. CO molecule. If comparing the binding energies of different structures, as it is done in the surface phase diagram, the change in the relative binding energies is even smaller. This can also directly be seen in Fig. A.4, where the surface phase diagram as discussed in Chapter 7 is shown for a planewave cutoff of $E^{\text{wf}}_{\text{max}} = 20\,\text{Ry}$ and $24\,\text{Ry}$. Only very small shifts in the phase boundaries can be observed. It is thus concluded

that a planewave cutoff of $E_{\mathrm{max}}^{\mathrm{wf}} = 20\,\mathrm{Ry}$ is sufficient for the problems discussed in the present work.

A.3 Molecular Binding Energies

In the present work the binding energies of three different molecules, O_2, CO and CO_2 are needed. Within periodic boundary conditions the molecules as well as the respective atoms have to be calculated in a 3-dimensional box surrounded by enough vacuum to avoid interactions between the periodic images. Since the atomic and molecular states do not have any dispersion a sampling of the Γ-point only is sufficient. This leaves as the most important parameters the muffin-tin radii R_{MT} and the planewave cutoff for the representation of the wave function in the interstitial, $E_{\mathrm{max}}^{\mathrm{wf}}$. The remaining parameters are equivalent to the ones discussed in Section A.1. In the following the convergence of the binding energies of the three molecules with respect to $E_{\mathrm{max}}^{\mathrm{wf}}$ will be discussed.

Oxygen

In addition to determining ΔE^{mol} (cf. Eq. (7.5)) the binding energy of the O_2 molecule is needed to calculate the total energy of O_2 for any arbitrary muffin-tin radius. Since total energies converge differently for different muffin-tin radii with respect to the chosen basis set, the total energies of a system calculated using different muffin-tin radii are only comparable, if all basis set parameters are fully converged. To calculate a binding energy as the difference of total energies it is thus much more convenient to use the same muffin-tin radii for each subsystem to obtain a much faster convergence. Also the binding energy of an oxygen atom on a surface with respect to an O_2 molecule in the gas phase can therefore be determined with a much smaller basis set, if the same muffin-tin radius is used for the oxygen in both system. Due to the bond length in the O_2 molecule the best muffin-tin radius is $R_{\mathrm{MT}}^{\mathrm{O}} = 1.1\,\mathrm{bohr}$. Smaller muffin-tin radii would require a higher $E_{\mathrm{max}}^{\mathrm{wf}}$, whereas large muffin-tin radii are simply not possible due to overlapping spheres. This restriction might impose rather unfavorable choices for the oxygen muffin-tin radius in other systems. To circumvent this problem the total energy of the oxygen molecule is expressed as

$$E_{\mathrm{O_2}}^{\mathrm{tot}} = 2E_{\mathrm{O}}^{\mathrm{tot}} + E_{\mathrm{O_2}}^{\mathrm{bind}} \quad . \tag{A.1}$$

The oxygen atom can then be calculated for any given value of $R_{\mathrm{MT}}^{\mathrm{O}}$ and together with the O_2 binding energy the total energy of the O_2 molecule can be determined.

To obtain the binding energy of the O_2 molecule the calculations are performed spin-polarized in a $(13 \times 14 \times 18)$ bohr supercell for the molecule, resp. a $(13 \times 14 \times 15)$ bohr supercell for the atom. The supercells are setup asymmetric to provide a proper occupation of the orbitals, i.e. in the case of an oxygen atom there are 4 valence electrons distributed in 3 p-orbitals, 3 electron spin up and one electron spin down.

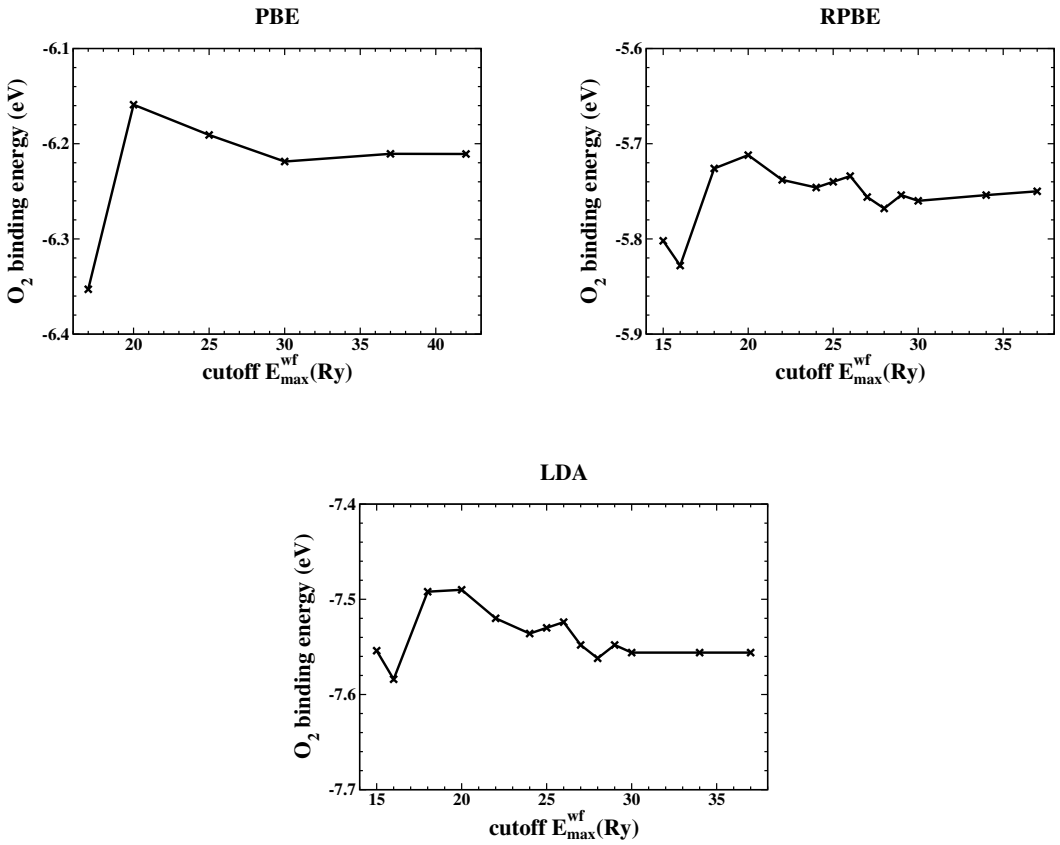

Figure A.5: Convergence of oxygen binding energy with respect to the cutoff of the planewave representation of the wave function in the interstitial for the PBE, RPBE and LDA exchange-correlation functional.

	$E_{O_2}^{\text{bind}}$	d_{O-O}
PBE	-6.20	2.301
RPBE	-5.75	2.303
LDA	-7.56	2.281
Exp. [11]	-5.17	2.282

Table A.4: Binding energies and bond lengths of the O_2 molecule calculated using the PBE, RPBE and LDA as exchange-correlation functional and a planewave cutoff of $E_{\text{max}}^{\text{wf}} = 37\,\text{Ry}$. The binding energies are given in eV, the bond lengths in bohr.

In a symmetric supercell the 3 p-orbitals would be degenerate and thus every p-orbital would be occupied with one electron spin up and 1/3 electron spin down.

In Fig. A.5 the convergence of the O_2 binding energy with respect to the planewave cutoff $E_{\text{max}}^{\text{wf}}$ is shown for all three exchange-correlation functionals, PBE, RPBE and LDA. By comparing the RPBE and LDA results it can be nicely observed that the

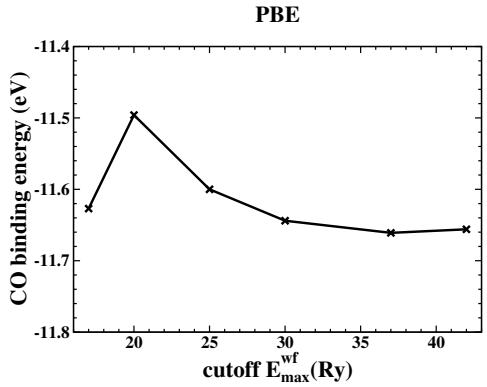

Figure A.6: Convergence of CO binding energy with respect to the cutoff of the planewave representation of the wave function in the interstitial for the PBE exchange-correlation functional

	$E_{\mathrm{CO}}^{\mathrm{bind}}$	$d_{\mathrm{C-O}}$
PBE	-11.65	2.151
RPBE	-11.20	2.158
LDA	-12.93	2.133
Exp. [11]	-11.16	2.132

Table A.5: Binding energies and bond lengths for the CO molecule calculated using the PBE, RPBE and LDA as exchange-correlation functional and a planewave cutoff of $E_{\mathrm{max}}^{\mathrm{wf}} = 37\,\mathrm{Ry}$. The binding energies are given in eV, the bond lengths in bohr.

convergence behavior is almost equivalent for the different exchange-correlation functionals. The same is also true for the PBE, which is not as obvious in Fig. A.5, since a different number of points has been calculated. For a planewave cutoff of $E_{\mathrm{max}}^{\mathrm{wf}} > 30\,\mathrm{Ry}$ the binding energies are almost constant for all three functionals.

For the best planewave cutoff of $E_{\mathrm{max}}^{\mathrm{wf}} = 37\,\mathrm{Ry}$ additionally the bond length of the O_2 molecule has been fully relaxed for each exchange-correlation functional. The binding energies and corresponding bond lengths are listed in Tab. A.4.

Carbon Monoxide

The CO molecule as well as the C and O atoms have been calculated in a $(13 \times 14 \times 15)$ bohr supercell using muffin-tin radii of $R_{\mathrm{MT}}^{\mathrm{O}} = R_{\mathrm{MT}}^{\mathrm{C}} = 1.0\,\mathrm{bohr}$. The remaining parameters are equivalent to the ones previously described for the O_2 molecule, except that the CO molecule does not have to be treated spin-polarized. The convergence behavior of the binding energy with respect to the planewave cutoff, $E_{\mathrm{max}}^{\mathrm{wf}}$, is shown in Fig. A.6 for the PBE exchange-correlation functional. Again the convergence behavior for the different exchange-correlation functionals is expected to be similar. To obtain highly converged results a planewave cutoff of $E_{\mathrm{max}}^{\mathrm{wf}} = 37\,\mathrm{Ry}$ is chosen for all

	$E_{CO_2}^{bind}$	d_{C-O}
PBE	-17.99	2.218
RPBE	-17.09	2.226
LDA	-20.43	2.202
Exp. [11]	-16.68	2.192

Table A.6: Binding energies and bond lengths for the CO_2 molecule calculated using the PBE, RPBE and LDA as exchange-correlation functional and a planewave cutoff of $E_{max}^{wf} = 37\,Ry$. The binding energies are given in eV, the bond lengths in bohr.

three functionals to calculate the binding energies and relaxed bond lengths listed in Tab. A.5.

Carbon Dioxide

To determine the binding energy of the CO_2 molecule muffin-tin radii of $R_{MT}^{O} = R_{MT}^{C} = 1.1\,bohr$ are used. The CO_2 molecule is treated non-spin-polarized in a $(13 \times 14 \times 20)\,bohr$ supercell, the O and C atom spin-polarized in $(13 \times 14 \times 15)\,bohr$ supercells. The remaining parameters are equivalent to the ones previously described for the O_2 molecule. Since the convergence behavior of the binding energy with respect to the planewave cutoff is expected to be similar to the previously discussed O_2 and CO molecules the calculations have only been performed for a planewave cutoff of $E_{max}^{wf} = 20\,Ry$ and $37\,Ry$. Increasing the planewave cutoff from $20\,Ry$ to $37\,Ry$ the change in the binding energies is already $\lesssim 0.1\,eV$ for all three functionals. The binding energies and respective bond lengths for $E_{max}^{wf} = 37\,Ry$ are listed in Tab. A.6.